

Fracture Prediction and Correlation of AlSi Hot Stamped Steels with Different Models in LS-DYNA[®]

G. Huang, H. Zhu, S. Sriram
ArcelorMittal Global R&D E. Chicago Center
Y. Chen, Z. C. Xia, O. Faruque
Ford Motor Company

Abstract

Reliable predictions of the fracture behavior in a crash event have become ever important in recent years as they will enable the reduction of physical prototype testing and the acceleration of vehicle development time while maintaining high safety standards. The increasing use of even stronger grades of Advanced High-Strength Steels (AHSS) such as hot-stamped boron steels provides particular challenges to fracture modeling due to their microstructures and processing conditions. This paper provides a brief description of the different fracture criteria and their implementation currently available in LS-DYNA to model ductile failure. The focus is the determination of parameters for selected fracture criteria for AlSi coated press-hardenable steels using calibration tests at the coupon level and supported by FEA simulations.

Introduction

Over the past two decades, design and analysis of automotive body structures have become heavily reliant on computational techniques owing to highly compressed design cycles. Prediction of crash performance at the component, sub-system and full vehicle level using LS Dyna for a number of loadcases to satisfy different regulatory requirements has become a core step in the design process. Simultaneously, there is considerable pressure on the automotive OEMs and their suppliers to meet the upcoming 2025 CAFÉ requirement for the vehicle fleet to achieve 54.5 MPG. To meet the regulations it is very important to ensure optimum designs coupled with appropriate materials that meet or exceed the mandated safety requirements.

To address current and future automotive design and manufacturability requirements, steel suppliers are continuing to develop products with higher strength and ductility to enable ease of manufacturability and still retain enough residual ductility for crash energy management. One particularly innovative product, USIBOR[®], developed by ArcelorMittal belongs to a class of products that are tailored to be stamped at high temperatures and then quenched in the die to achieve a fully martensitic microstructure. These products are very effective in obtaining complex part shapes coupled with very high strength (up to 1500 MPa) in the part without any springback. In addition, USIBOR[®] is coated with Aluminum and Silicon which result in the formed product being scale-free after hot stamping. These product features make USIBOR[®] an attractive steel product to be used in automotive body structures.

With the increase in the number of higher strength AHSS parts in safety-critical regions in the body structure coupled with strong reliance on FEA during the design process, it is critical to ensure prediction accuracy when modeling crash loading sequences. Modeling of failure and fracture and subsequent use in FEA has become more and more sophisticated incorporating newer and improved understanding of the phenomenon. Fracture behavior of materials has been of interest for a very long time. In general fracture behavior is classified as brittle or ductile with

ductile failure preceded by significant plastic flow in the material. For ductile fracture, before material separation at significant plastic strains, voids are nucleated predominantly at the interface of the harder phase particles with the softer matrix. As deformation proceeds, these voids grow and coalesce while at the same time increasing the local stresses. The process of void nucleation and growth is a typical characteristic of ductile fracture. The earliest criterion for ductile fracture was based on maximum shear stress being achieved for the material during loading [1]. An improvement on this criterion was developed by Mohr and Coulomb [1] who proposed that failure occurred when a certain combination of tensile and shear stress was reached during loading. A more general criterion was proposed by Johnson and Cook [2] who conducted experiments on several materials and established the relationship between equivalent strain at fracture as a function of the triaxiality factor during loading. The triaxiality factor is the ratio of the trace of the stress tensor (hydrostatic pressure) to the vonMises effective stress. The fundamental relationship of the fracture strain to the triaxiality factor was characterized further as a function of strain rate and temperature. Separately, the geophysics and the soil mechanics community has long realized the importance of the third invariant of the deviatoric stress tensor and its role in fracture behavior. In the Haigh-Westergaard stress space, this is often represented as the Lode angle. Recently, Xue-Wierzbicki model [3] and modified Mohr-Coulomb model [4] have been proposed to account for dependence of triaxiality factor and the Lode angle for the equivalent fracture strain for a number of metallic materials, and promising results of fracture prediction were obtained from application of their fracture models. Void coalescence and growth has also been studied extensively and there are some well known articles to characterize void nucleation and grown behavior [5, 6]. In terms of prediction of fracture, the MATFEM Co. developed CRACHFEM which is used in several simulation software. CRACHFEM uses two mechanisms for fracture (a) void nucleation and coalescence and (b) shear fracture. They use expressions for these two competing mechanisms and whichever reaches the limit strain first, fracture is said to occur by that mechanism. In addition to characterizing fracture behavior under different loading conditions, some work has also been done in postulating material damage. Obviously, since damage cannot be directly measured, empirical expressions are used to describe damage behavior. More recently the GISSMO approach [7] where the damage parameter can be coupled with stress calculation and including the fracture strain dependence on triaxiality and the Lode angle parameter has been proposed.

Thus, there are a number of different approaches to describing ductile failure in metals and their implementation in commercial FEA programs such as LS Dyna. This paper describes some details of the different fracture models, their implementation and the calibration tests required to describe the fracture behavior. All the testing and fracture characterization were conducted on USIBIOR[®] which is expected to be widely used in automotive body structures in the short to mid-term.

Different Fracture Models and Implementation in LS Dyna

Three fracture models are used in this study for fracture prediction; they are GISSMO, MIT Modified Mohr-Coulomb (MMC) model and Johnson-Cook model. While GISSMO and Johnson-Cook model have been implemented in LS-DYNA as *MAT 224 and *MAT_ADD_EROSION, MIT MMC model has not been commercially implemented in LS-DYNA, but can be used through *MAT 224 or *MAT_ADD_EROSION with tabulated fracture data for input. The common feature of the three different models is that fracture is

assumed to depend on the hydrostatic pressure (triaxiality) and Lode parameter. Numerous studies [3-11] have discovered that damage and fracture initiation for ductile materials depends both on hydrostatic pressure and shear stress. To appropriately predict fracture of AHSS during manufacturing and crash events, it is essential that both parameters be considered as critical material inputs for simulation. For mathematical convenience, the hydrostatic pressure and shear stress (deviatoric stress) are usually normalized as non-dimensional variables, shown in Eqs. (1) and (2).

$$\eta = \frac{-p}{\bar{\sigma}} = \frac{\frac{1}{3}(\sigma_1 + \sigma_2 + \sigma_3)}{\bar{\sigma}} \tag{1}$$

$$\xi = \frac{27 J_3}{2 \bar{\sigma}^3} \tag{2}$$

Where η and ξ are stress triaxiality (normalized pressure) and normalized third deviatoric invariant, respectively; p is hydrostatic pressure, σ_1 , σ_2 and σ_3 are the principal stress components, J_3 is the third invariant of deviatoric stress tensor, and $\bar{\sigma}$ (for isotropic materials) is the equivalent stress which is represented in Eq. (3).

$$\bar{\sigma} = \frac{\sqrt{2}}{2} \sqrt{(\sigma_1 - \sigma_2)^2 + (\sigma_2 - \sigma_3)^2 + (\sigma_3 - \sigma_1)^2} \tag{3}$$

The normalized third deviatoric invariant, ξ , was found to be related to Lode angle, θ [9].

$$\cos(3\theta) = \xi \tag{4}$$

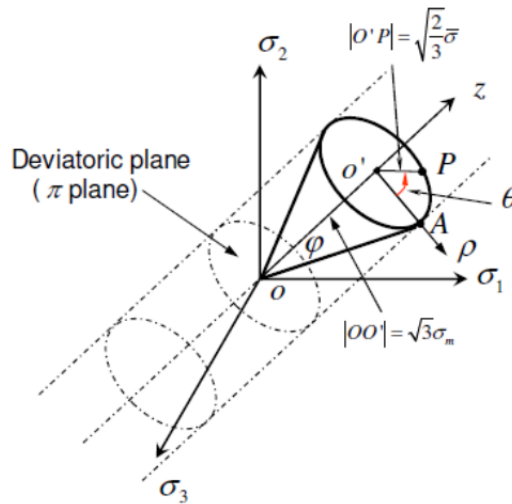


Figure 1: Representation of Lode angle (θ), hydrostatic pressure ($-\sigma_m$), and effective stress ($\bar{\sigma}$) in spherical coordinate system

Conceptually, the range of θ is $[0, \pi/3]$, as schematically illustrated in Fig. 1. To normalize the Lode angle into $[-1, 1]$, Eq. (4) is changed into:

$$\bar{\theta} = 1 - \frac{2}{\pi} \arccos \xi \tag{5}$$

The relation [12] between principal stress components and the two important variables (η & ξ) are shown in Eq. (6).

$$\begin{bmatrix} \sigma_1 \\ \sigma_2 \\ \sigma_3 \end{bmatrix} = \begin{bmatrix} [\eta + \frac{2}{3} \cos(\theta)] \bar{\sigma} \\ [\eta + \frac{2}{3} \cos(\theta - \frac{2}{3} \pi)] \bar{\sigma} \\ [\eta + \frac{2}{3} \cos(\theta + \frac{2}{3} \pi)] \bar{\sigma} \end{bmatrix} \quad (6)$$

From Eq. (6) it is clear that all stress components can be represented by η and θ . Furthermore, if the constitutive relation (between equivalent stress and strain, i.e. $\bar{\sigma}$ and $\bar{\varepsilon}$) is known, the formulation in stress space can be converted to a space composed of strain, η and θ .

Modified Mohr-Coulomb Model

The modified Mohr-Coulomb model developed by MIT in 2007 was based on Mohr-Coulomb fracture mechanism [4]. The original Mohr-Coulomb model assumed the fracture initiation occurs when the combination of shear stress and friction reaches a critical value, as depicted in Eq. (7).

$$(\tau + f\sigma_n)_{\max} = C \quad (7)$$

where τ is the shear stress, σ_n is the normal stress, f is the friction coefficient of inner body and C is a constant. With Lagrangian multiplier to find the maximum value, Eq. (7) can be changed to

$$(\sqrt{1+f^2} + f)\sigma_1 - (\sqrt{1+f^2} - f)\sigma_3 = C \quad (8)$$

Theoretically, Eq. (7) or Eq. (8) should be readily applicable and implemented in FEA in a straightforward manner. However, due to the fact that all variables are related to stress which is very difficult to measure during material calibration for the criterion, Eqs. (7) and (8) are not convenient for application in reality. However, by use of Eq. (6), Mohr-Coulomb model can be easily formulated in the space of strain, η and θ ,

$$F(\bar{\varepsilon}) = C \left/ \left[\frac{\sqrt{1+f^2}}{3} \cos\left(\theta - \frac{\pi}{6}\right) + f \left(\eta - \frac{1}{3} \sin\left(\theta - \frac{\pi}{6}\right) \right) \right] \right. \quad (9)$$

To improve accuracy of plasticity prediction, a generalized hardening rule considering the effect of triaxiality and Lode angle was proposed by Bai and Wierzbicki [4],

$$F(\bar{\varepsilon}) = \bar{\sigma} = K \bar{\varepsilon}^n \left[C_\theta^s + \frac{\sqrt{3}}{2-\sqrt{3}} (1 - C_\theta^s) \left(\sec\left(\theta - \frac{\pi}{6}\right) - 1 \right) \right] \quad (10)$$

where C_θ^s is a parameter to describe the Lode angle dependence. Plugging Eq. (10) into (9) and using Eq. (5) leads to the MMC fracture criterion [4]

$$\bar{\varepsilon}_f = \left\{ \frac{K}{C} \left[C_\theta^s + \frac{\sqrt{3}}{2-\sqrt{3}} (1 - C_\theta^s) \left(\sec\left(\frac{\pi\bar{\theta}}{6}\right) - 1 \right) \right] \left[\frac{\sqrt{1+f^2}}{3} \cos\left(\frac{\pi\bar{\theta}}{6}\right) + f \left(\eta + \frac{1}{3} \sin\left(\frac{\pi\bar{\theta}}{6}\right) \right) \right] \right\}^{-\frac{1}{n}} \quad (11)$$

When $C_\theta^s=1$, Eq. (11) leads to the original Mohr-Coulomb model with power law hardening, $\bar{\sigma} = K\bar{\varepsilon}^n$, where, $\bar{\varepsilon} = \varepsilon_0 + \varepsilon_p$. In addition to fracture initiation, MMC model also prescribed the rule for damage evolution. The incremental damage is written as

$$dD = \frac{d\varepsilon_p}{\varepsilon_f(\eta, \xi)}. \quad (12)$$

Fracture is assumed to initiate when D accumulates to 1. However, MMC model allows D to exceed unity so as to predict further softening of material by gradually propagating the crack within the element. The reduction of deformation resistance or stress is described as

$$\hat{\sigma} = \sigma \left(\frac{D_c - D}{D_c - D_0} \right)^m, \quad (13)$$

Where $\hat{\sigma}$ is the true stress, and D_c is the critical damage when the stress drops to zero and D_0 is the initial damage value when softening starts. To cope with the variation of stress triaxiality and lode angle, averaged value in integral form is applied in MMC model:

$$\begin{cases} \eta_{ave} = \frac{1}{\varepsilon_f} \int_0^{\varepsilon_f} \eta(\bar{\varepsilon}) d\bar{\varepsilon} \\ \xi_{ave} = \frac{1}{\varepsilon_f} \int_0^{\varepsilon_f} \xi(\bar{\varepsilon}) d\bar{\varepsilon} \end{cases} \quad (14)$$

GISSMO

GISSMO is a phenomenological fracture model [7, 13-15] which takes into account the damage evolution and fracture dependence on triaxiality and Lode parameter. The damage factor D is assume to accumulate exponentially as

$$D = \left(\frac{\varepsilon}{\varepsilon_f} \right)^{n'}. \quad (15)$$

Taking the derivative leads to the incremental damage as function of only current damage factor, incremental plastic strain, and failure strain:

$$dD = \frac{n'}{\varepsilon_f} \left(\frac{\varepsilon}{\varepsilon_f} \right)^{n'-1} d\varepsilon_p = \frac{n'}{\varepsilon_f(\eta, \xi)} D^{\frac{n'-1}{n'}} d\varepsilon_p. \quad (16)$$

It should be noted that when $n'=1$, Eq. (16) is equivalent to Eq. (12) of MMC model for incremental damage. From Eq. (16), the damage evolution can be expressed in the form of

$$D_{total} = \int \frac{n'}{\varepsilon_f(\eta, \xi)} D^{\frac{n'-1}{n'}} d\varepsilon_p = \int f(D, \eta, \xi) d\varepsilon_p. \quad (17)$$

Theoretically the upper limit of total damage is 1. However, it can be prescribed as some number between 0 and 1, depending on the material and loading condition. For the present study, the failure is assumed to occur when total damage reaches 1. In the GISSMO model, when the plastic strain reaches a certain value such that threshold of damage D_{crit} is triggered, the true stress is reduced, i.e., softening being in effect, based on

$$\sigma^* = \sigma \left(1 - \left(\frac{D - D_{crit}}{1 - D_{crit}} \right)^m \right), \quad (18)$$

where D_{crit} can be the damage at time of instability or a prescribed constant from calibration. Thereafter, the damage accumulates according to Eq. (17) until it reaches value of 1, and element is deleted. During plastic deformation where the loading is not proportional, the triaxiality or Lode angle is function of strain instead of a constant. For calibration and application of (17), a weighting function is used to determine the triaxiality/Lode angle as representation of the history:

$$\begin{cases} \eta_w = \frac{1}{D} \int f(D, \eta, \xi) \eta d\varepsilon_p = \frac{1}{D} \int \frac{n'}{\varepsilon_f(\eta, \xi)} D^{\frac{n'-1}{n'}} \eta d\varepsilon_p \\ \xi_w = \frac{1}{D} \int f(D, \eta, \xi) \xi d\varepsilon_p = \frac{1}{D} \int \frac{n'}{\varepsilon_f(\eta, \xi)} D^{\frac{n'-1}{n'}} \xi d\varepsilon_p \end{cases} \quad (19)$$

Johnson-Cook Model

The Johnson-Cook Model [2] assumed that strain at fracture monotonically decreases with triaxiality, as depicted in Eq. (20).

$$\varepsilon_f = C_1 + C_2 e^{C_3 \eta} \quad (20)$$

The damage is defined as

$$D = \int \frac{d\varepsilon_p}{\varepsilon_f(\eta)} \quad (21)$$

The fracture is assumed to initiate when D reaches 1.

Calibration Tests and Parameter Identification

Experiments

The tensile properties of the material are displayed in Table 1. In order to achieve different stress states with different combinations of stress triaxiality and Lode angles, 5 different lab tests were chosen to for calibration of three fracture models. The tests covered the stress states of uniaxial tension, stretching (between stress states of uniaxial and plane strain), plane strain, biaxial and equibiaxial stretching. A schematic of test samples for the 5 individual tests are shown in Fig. 2, where the cut-out test denotes the test in the drawing condition.

Table 1: Tensile properties of tested USIBOR[®]

Thickness (mm)	Coating	Yield strength (MPa)	Tensile strength (MPa)	Uniform elongation	Total elongation
1.6	AlSi	983	1497	0.043	0.066

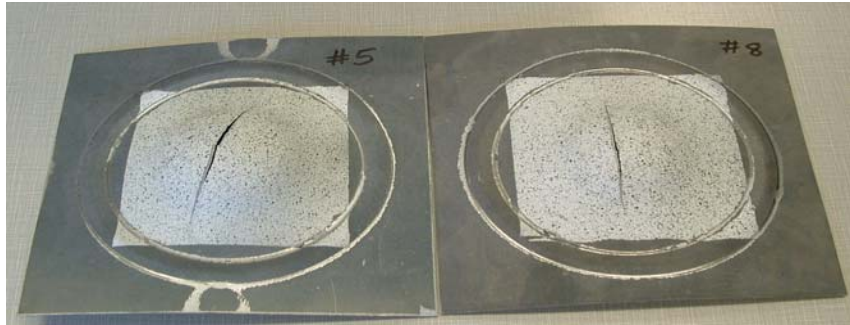


Figure 4: Example of tested samples from equibiaxial tests

Measurement results

In order to calibrate the three fracture criteria, fracture strains for each test has to be measured. Digital Image Correlation (DIC) was used for strain measurement in the 5 calibration tests [16]. Fig. 3 illustrated the DIC system used during the calibration tests, where 2-D DIC was used in tensile tests on specimens shown in Fig. 2 (a) and (b), and 3-D DIC was used in Dome tests (Fig. 2 (c)-(e)). Images of specimens were acquired at a speed of 15 frames /sec throughout the entire testing process, and were analyzed to determine the history of strain at local area of fracture occurrence. Fig. 4 shows an image of equibiaxial samples with fracture after testing. As one of the important material inputs for CAE simulation of fracture, stress-strain data have to be determined from uniaxial tensile tests. The extended stress-strain curves were extracted based on the previously developed method using DIC [17], and plotted in Fig. 5. For comparison, other than T direction (tensile direction) the stress-strain curves for longitudinal (L) direction were also determined. As shown in Fig. 5, the stress-strain curves in L direction are close to those in T direction, indicating the anisotropy is not significant for USIBOR. The fracture strains measured from uniaxial tests are shown in Table 2. The measured fracture strains for other calibration tests are listed in Tables 3-6. For all strain measurements in this study, a gauge length of 1mm was applied, and the fracture strain was measured at the moment immediately prior to fracture. In order to assure the fracture initiated away from edges to avoid the complication caused by edge fracture, verification was conducted with the help of images and results of strain contour. To illustrate, the image with major strain contour right before fracture was shown in Fig. 6 for cut-out test and plane strain test, respectively; it can be seen that, with the maximum strain being close to the center of specimen width right before fracture, clearly the fracture is not edge fracture.

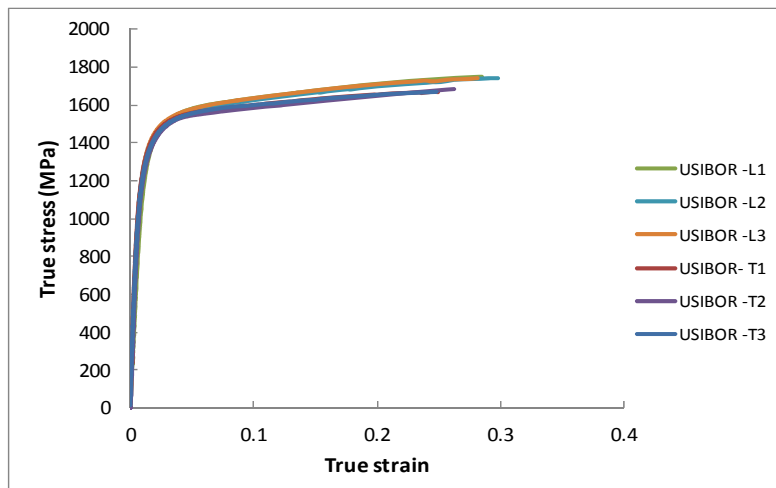


Figure 5: Extended stress-strain curves of 1.6mm USIBOR

Table 2: Fracture strains measured from uniaxial tensile tests

Repeat	Major strain	Minor strain	Effective strain
Test 1	0.355	-0.228	0.360
Test 2	0.335	-0.212	0.339
Test 3	0.326	-0.241	0.338
Average	0.339	-0.227	0.346

Table 3: Fracture strains from Cut-out tests

Repeat	Major strain	Minor strain	Effective strain
Test 1	0.183	-0.0338	0.195
Test 2	0.189	-0.0413	0.199
Test 3	0.2168	-0.0472	0.228
Average	0.196	-0.0408	0.207

Table 4: Fracture strains from plane strain tests

Repeat	Major strain	Minor strain	Effective
Test 1	0.115	0.003	0.134
Test 2	0.114	0.011	0.139
Test 3	0.101	0.013	0.125
Average	0.118	0.009	0.133

Table 5: Fracture strains from biaxial stretch tests

	Major strain	Minor strain	Effective
Test 1	0.141	0.0722	0.217
Test 2	0.162	0.0797	0.247
Average	0.152	0.0760	0.232

Table 6: Fracture strains from equibiaxial tests

Repeat	Major strain	Minor strain	Thinning	Effective	Original thickness	Final thickness	Measured thinning
Test 1	0.134	0.105	-0.239	0.240	1.594	1.250	-0.243
Test 2	0.152	0.133	-0.285	0.285	1.580	1.226	-0.254
Test 3	0.129	0.11	-0.239	0.239	1.594	1.248	-0.245
Average	0.138	0.116	-0.25433	0.255	1.589	1.241	-0.247

In order to validate the strain measurement method using DIC, thinning measurement using point micrometer was conducted to cross-check the fracture strains from equibiaxial tests. Table 6 includes the thinning strains measured after tests, and the thinning strains calculated from major and minor strains using DIC and volume conservation. From comparison, the thinning strains determined using DIC are in very good agreement with those using the point micrometer, indicating the measurement using DIC is valid and accurate.

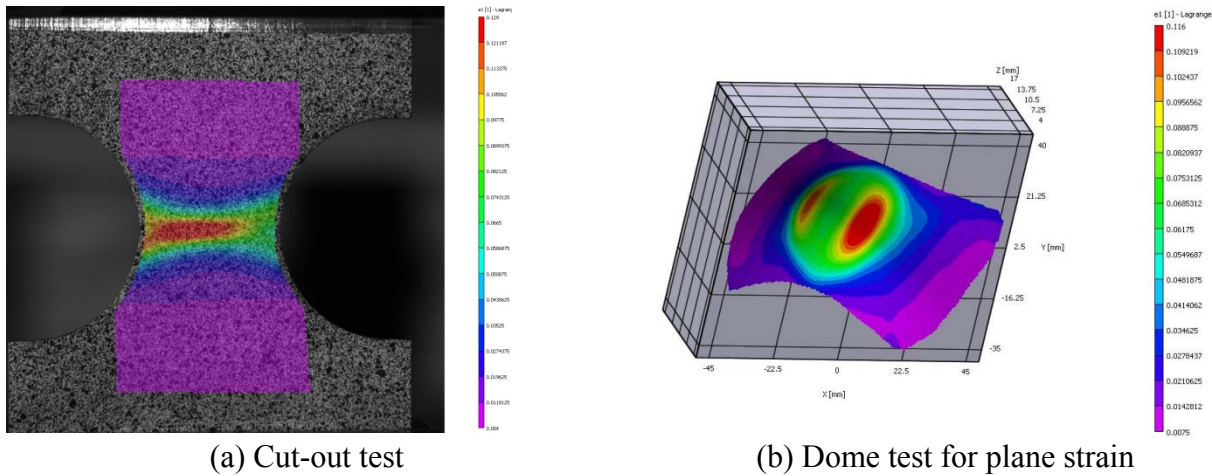
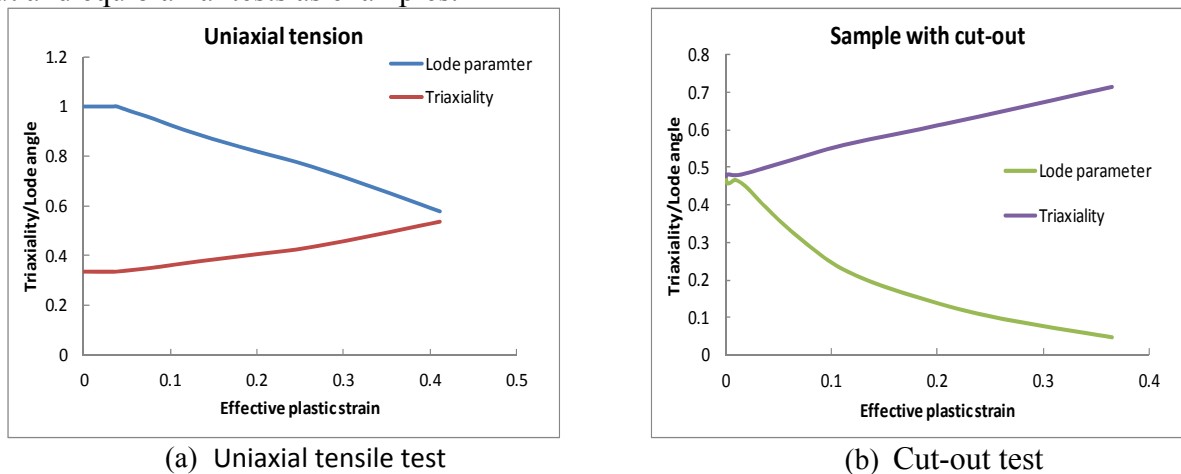
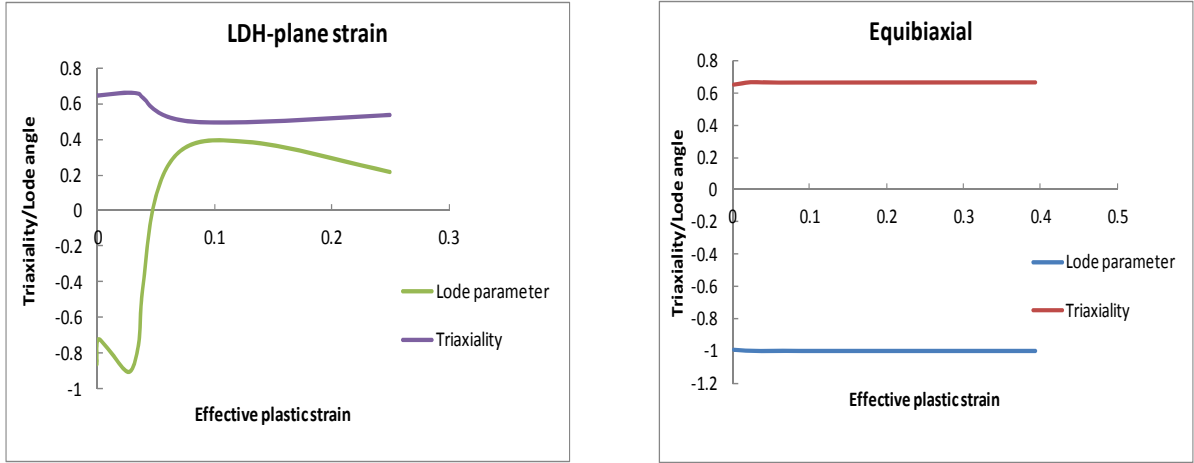


Fig. 6: Examples of strain contour from calibration tests showing fracture initiation not on edge

Parameter identification process for fracture models

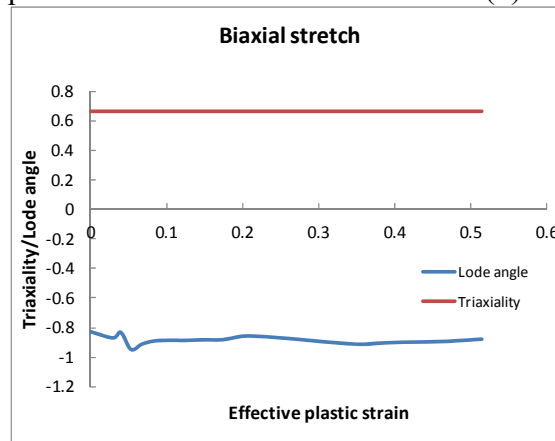
FEA simulations were conducted on the 5 calibration tests. Solid elements with an element size of 0.2 mm in the plane and in thickness direction was used in critical area of fracture occurrence. Since FEA was aimed at parameter identification, no fracture criterion was applied. From the output of the critical element where the fracture was initiated (based on the experimental observation), the stress triaxiality and Lode angle were extracted for individual calibration tests. Thereafter, the parameters for 3 different fracture models can be determined to generate the fracture surface represented by the fracture strain as a function of triaxiality and Lode angle. The output of stress triaxiality and Lode angles from simulations are shown in Fig. 7 for different calibration tests. The effective plastic strain (ϵ_{eff}) contour of specimen is shown in Fig. 8 for cut-out and equibiaxial tests as examples.





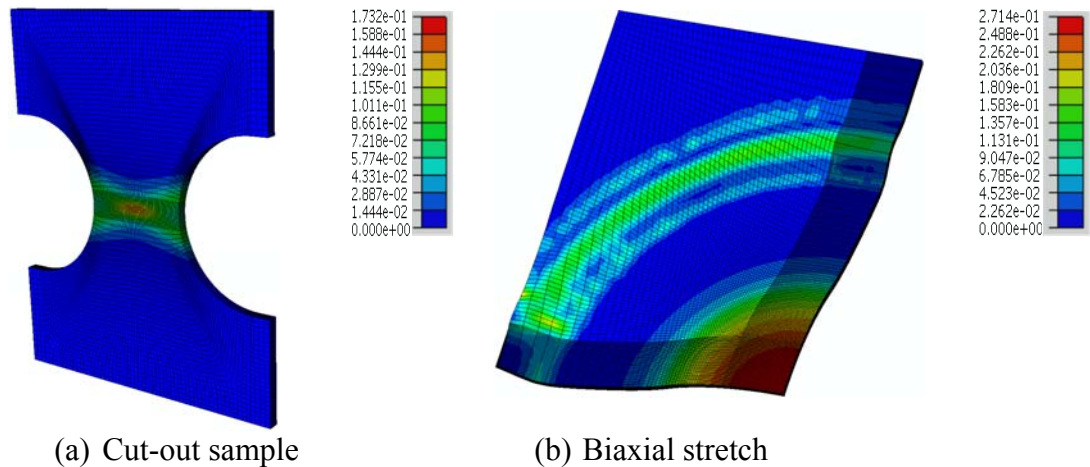
(c) Dome test for plane strain

(d) Equibiaxial test



(e) Biaxial stretch test

Figure 7: Stress triaxiality and Lode angle as functions of effective plastic strain



(a) Cut-out sample

(b) Biaxial stretch

Figure 8: Examples of ϵ_{eff} contour (right before fracture) from simulation

To verify the measurement from the calibration tests, the strain from simulation at moment of displacement at fracture was compared with fracture strain measured experimentally. As shown in Table 7, the results of fracture strain from experiment and simulation are very close to each

other, implying that the simulation with the measured fracture strain used later in fracture criteria is valid for fracture prediction for the calibration tests.

Table 7: Comparison of fracture strains from experiment and simulation

Calibration test	Effective fracture strains				
	Uniaxial tensile	Cut-out	Plane strain	Biaxial stretch	Equibiaxial
Experiment	0.346	0.189	0.125	0.247	0.24
Simulation	0.368	0.173	0.119	0.265	0.238

Calibration results

MMC model

To calibrate MIT MMC model to determine parameters in Eq. (11), the stress strain curves has to be fitted using Swift law first to obtain value of K and n . The curve fitting result is shown in Fig. 9. Meanwhile, equation(14) was used to calculate the representative stress triaxiality and Lode angle from the data history described in Fig. 7. The calculated triaxiality and Lode angle with the corresponding fracture strain for individual test is summarized in Table 8. To solve the rest of parameters, C , f , and C_θ^s , an optimization code using MATLAB was developed to identify the best-fit parameters from minimizing the error between experimental data (Table 8) and Eq. (11). The determined MMC parameters are shown in Table 9. With the identified parameters plugged back into Eq. (11), the fracture surface as a function of triaxiality and Lode angle was plotted, as shown in Fig. 10.

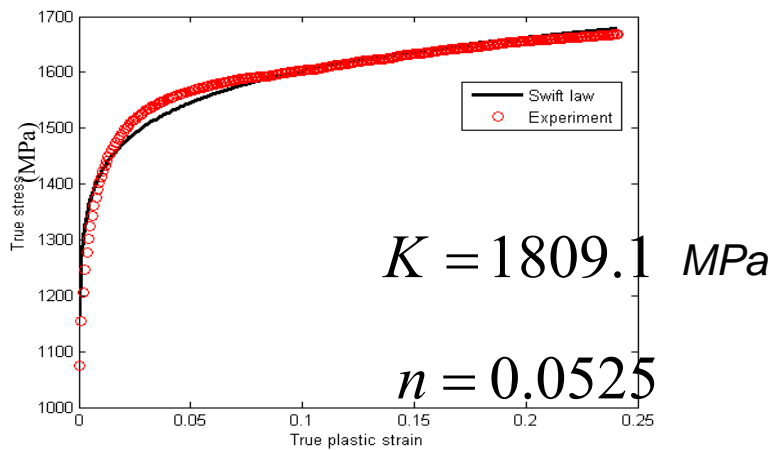


Figure 9: Curve fitting of USIBOR stress-strain data using Swift law

Table 8: Results of fracture strain as function of triaxiality and Lode angle (MMC)

	Triaxiality	Lode angle	Fracture strain
Uniaxial	0.3789	0.8389	0.346
Cut-out	0.5372	0.294851	0.207
Plane strain	0.5651	0.04	0.133
Biaxial	0.645	-0.87	0.232
Equi-biaxial	0.6624	-0.9989	0.255

Table 9: Parameters identified for MMC model

	K (MPa)	n	ϵ_0	f	C (MPa)	C_θ^s
Parametric value	1809.1	0.0525	0	0.1368	1000	0.9223

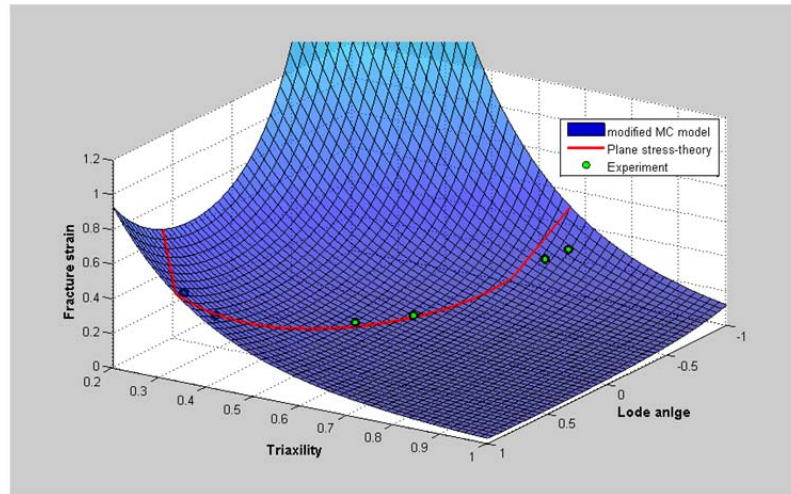


Figure 10: Fracture surface of 1.6mm USIBOR by MMC model after calibration

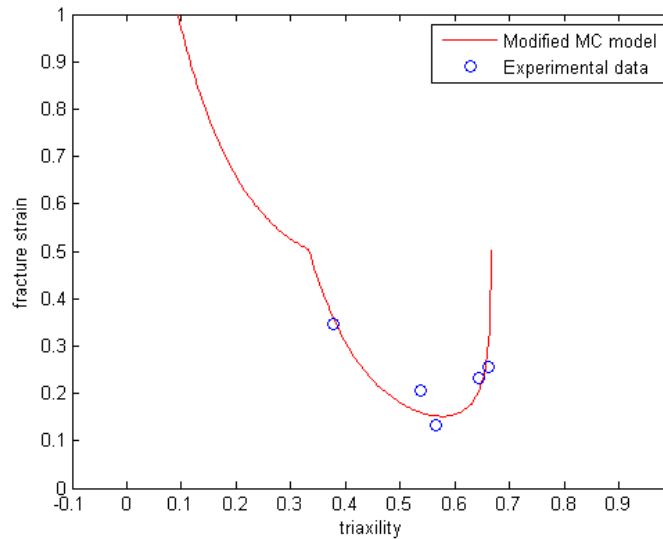


Figure 11: Fracture strain as function of triaxiality

For the case of plane stress, a relationship was found between triaxiality and Lode angle [3]:

$$\xi = \cos(3\theta) = -\frac{27}{2} \eta \left(\eta^2 - \frac{1}{3} \right). \tag{22}$$

With Eq. (22), fracture strain is only dependent on triaxiality or Lode angle in plane stress case. The resulting locus of fracture strain for the special case of plane stress is included in Fig. 11.

To utilize the calibrated MMC model for fracture prediction with *MAT 224 or *MAT_ADD_EROSION in LS-DYNA, the fracture surface represented by Eq. (11) was

converted to tabulated data of fracture strain with respect to triaxiality and Lode angle in discrete form.

GISSMO

Part of the calibration process for GISSMO is similar to MMC. Eq. (19) with the weighting function applied to calculate the representative triaxiality and Lode parameter from their history determined from simulation. Based on the recommendation from literature, the exponent $n=2$ was used. The resulting representative triaxiality and Lode parameter and the experimental fracture strain of each calibration test are show in Table 10.

It should be noted that GISSMO has no close-form solution for fracture strain surface. Therefore, the fracture strain surface has to be generated through interpolation of the discrete data points existing of fracture strain with respect to triaxiality and Lode angle in 3-D space. Based on the assumption that for a fixed Lode angle the fracture strain is decreasing with increasing triaxiality, the 3-D contour of fracture strain was formed via interpolation with exponential function. The result of fracture strain surface is shown in Fig. 12.

Table 10: Result of fracture strain as function of triaxiality and Lode angle (GISSMO)

	Triaxiality	Lode angle	Fracture strain
Uniaxial	0.41391	0.802821	0.346
Cut-out	0.5372	0.232585	0.207
Plane strain	0.58	0.06199	0.133
Biaxial	0.652254	-0.8731	0.232
Equi-biaxial	0.663424	-1	0.255

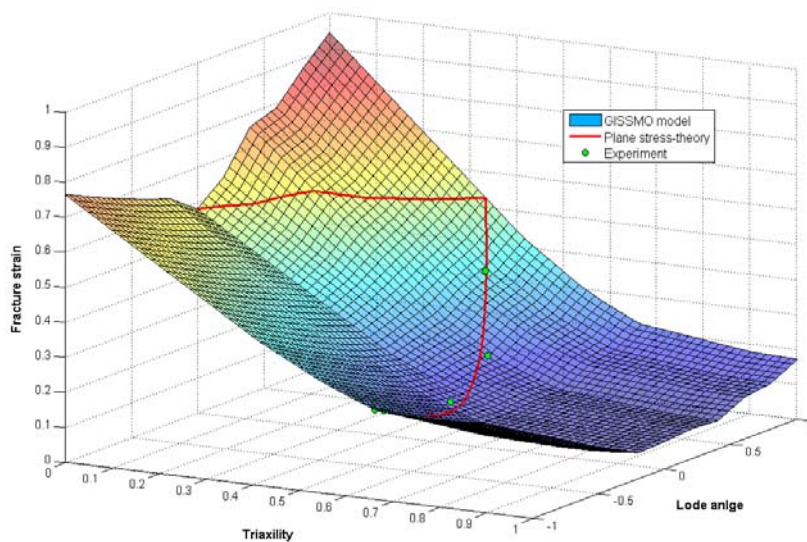


Figure 12: Fracture surface of 1.6mm USIBOR by GISSMO model after calibration

Johnson-Cook model

In this study, the Johnson-Cook fracture model was used in its original form as shown Eq. (20), which is independent of Lode angle. Therefore, only data of fracture strains and triaxiality from calibration tests to identify the parameters. The representative fracture strain and corresponding

triaxiality were fitted with Eq. (20) using nonlinear regression with MATLAB code. The results of curve fitting and determined parameters are shown in Fig. 13.

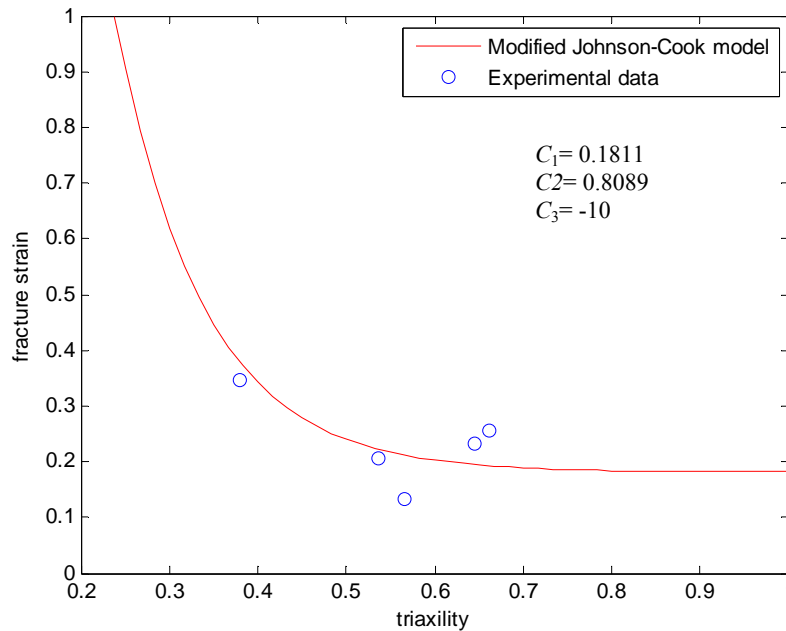
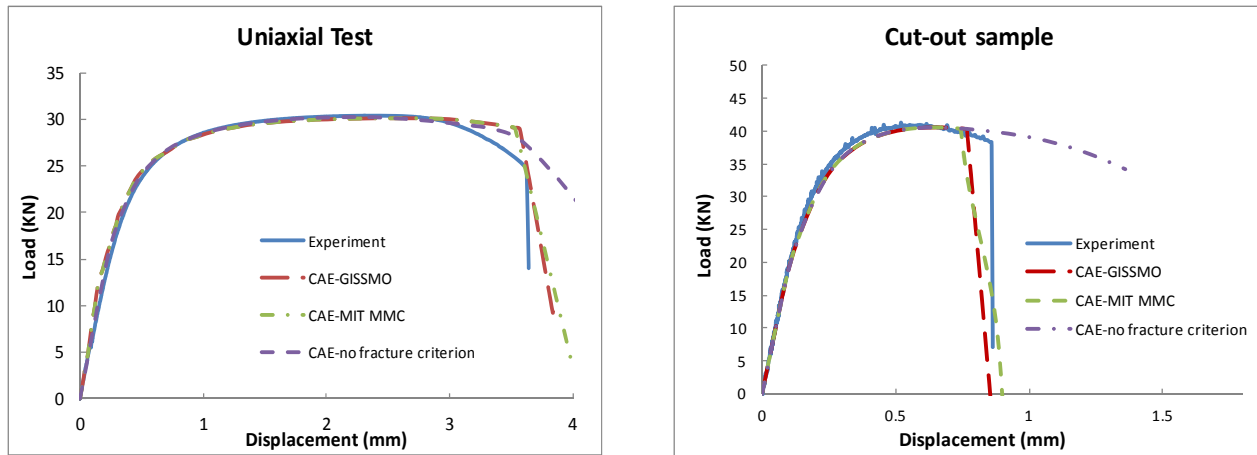


Figure 13: Fracture strain as function of triaxiality by Johnson-Cook model after calibration

Load-displacement data verification

The CAE simulations were conducted using a few fracture criteria with the material parameters/tabulated data from calibration process. The load displacement data were extracted from the simulations and compared with the experimental data to verify the fracture models applied. Fig. 14 shows the load-displacement curves from simulations using GISSMO and MIT MMC, and without any fracture criterion for uniaxial test and test on cut-out specimen, as some examples. The comparisons from Fig. 14 indicate that the load-displacement curves from simulations using GISSMO and MMC are close to those from experiment all along the test process, implying that the two criteria are able to reasonably predict the fracture initiation. Also plotted in Fig. 14 are the load-displacement curves from simulations without fracture criterion, it can be apparently seen that without applying fracture criterion the simulation was not predicting any substantial load drop caused by fracture, even though the results before fracture very good agreement with experimental data.



(a) Uniaxial test
(b) Cut-out test
Figure 14: Load-displacement data from simulation (without fracture criterion)

Conclusions

Three fracture criteria, MIT MMC, GISSMO and Johnson-Cook models, were discussed in terms of their application in fracture prediction of AHSS through LS-DYNA. Five tests with different stress states were used in calibration of the 3 models to determine the fracture surface (locus) used in LS-DYNA material card; the FEA simulation was conducted to determine the material parameters and correlate to experimental data. Meanwhile, the FEA simulation with implemented fracture models was also performed on the calibration tests and compared to experiment to verify applicability of the fracture models.

References

1. Rossmann H.P. Fracture research in retrospect - an anniversary volume in honor of George R. Irwin's 90th birthday, chapter: The struggle for recognition of engineering fracture mechanics, pages 37–93. A. A. Balkema Publishers, Rotterdam, 1997
2. Johnson G. R. and Cook W. H. "Fracture Characteristics of Three Metals Subjected to Various Strains, Strain Rates, Temperature and Pressures," *Engineering Fracture Mechanics*, vol. 21, No. 1, pp. 31-38, 1985.
3. Wierzbicki T. and Xue L. "On the Effect of the Third Invariant of the Stress Deviator on Ductile Fracture," *Impact and Crashworthiness Lab Report #136*.
4. Bai, Y. and Wierzbicki, T., "A new model of metal plasticity and fracture with pressure and Lode dependence," *International Journal of Plasticity*, 24, 1071–1096, 2008.
5. McClintock F. A. "A criterion for ductile fracture by growth of holes," *Trans. ASME. Journal of Applied Mechanics*, 35:363–371, 1968.
6. Rice J. R. and Tracey D. M. "On the ductile enlargement of voids in triaxial stress fields", *Journal of the Mechanics and Physics of Solids*, 17:201–217, 1969.
7. Effelsberg J., Haufe A., Feucht M., Neukamm F., and Du Bois P. Du, "On parameter identification for the GISSMO damage model," 12th International LS-DYNA Users Conference, Dearborn, June 2012.
8. McClintock, F.A., "Slip line fracture mechanics: A new regime of fracture mechanics," *Fatigue and Fracture Mechanics*, 33, ASTM STP-1417, West Conshohocken, PA; 2002.

9. Wierzbicki, T.; Bao, Y.; Lee, Y. and Bai Y., “Calibration and evaluation of seven fracture models,” *International Journal of Mechanical Sciences*, vol. 47, 719-743, 2005.
10. Lou, Y. and Huh, H., “Extension of a shear-controlled ductile fracture model considering the stress triaxiality and the Lode parameter”. *International Journal of Solids and Structures*, 50, pp. 447-455, 2013.
11. Li, Y. and Wierzbicki, T. “Prediction of plane strain fracture of AHSS sheets with post-initiation softening,” *International Journal of Solids and Structures*, 47, pp. 2316-2327, 2010.
12. Nayak, G.C. and Zienkiewicz, O.C., “Convenient forms of stress invariants for plasticity”, *Proceedings of the ASCE Journal of the Structural Division*, vol. 98, no. ST4, 949–954, 1972.
13. Neukamm, F., Feucht, M. and Haufe A., “Consistent damage modeling in the process chain of forming to crashworthiness simulations,” *LS-DYNA Anwenderforum*, 2008.
14. Neukamm, F., Feucht, M., and Haufe A., “Considering damage history in crashworthiness simulations,” 7th *European LS-DYNA Conference*, 2009.
15. Basaran, M., Wolkerlin, S.D., Feucht, M., Neukamm, F., Weichert, D., “An Extension of the GISSMO Damage Model Based on Lode Angle Dependence,” *LS-DYNA Anwenderforum*, Bamberg 2010.
16. Huang, G., Yan, B. and Zhu, H., “Measurement of fracture strains for advanced high strength steels using digital image correlation,” *SAE Paper 09M-1174*, 2009.
17. Huang, G., Zhu, H., and Yan, B., “A novel approach for generating a full-range tensile stress-strain curve,” *SAE Paper 09M-0172*, 2009.